



# Synthesis and molecular docking of hybrids ionic azole Schiff bases as novel CDK1 inhibitors and anti-breast cancer agents: *In vitro* and *in vivo* study



Waleed M. Serag<sup>a</sup>, Faten Zahran<sup>b</sup>, Yasmin M. Abdelghany<sup>a</sup>, Reda F.M. Elshaarawy<sup>a,c,\*</sup>, Moustafa S. Abdelhamid<sup>b</sup>

<sup>a</sup> Chemistry department, Faculty of Science, Suez University, Suez 43533, Egypt

<sup>b</sup> Biochemistry Division, Chemistry Department, Faculty of Science, Zagazig University, Egypt

<sup>c</sup> Institut für Anorganische Chemie und Strukturchemie, Heinrich-Heine Universität Düsseldorf, Düsseldorf, Germany

## ARTICLE INFO

### Article history:

Received 7 June 2021

Accepted 3 July 2021

Available online 7 July 2021

### Keywords:

Ionic vanillyl-azole-schiff bases

Molecular docking

*In vitro* and *in vivo* Cytotoxicity

Flow-cytometry

PAPR and VEGF

## ABSTRACT

Three new hybrid ionic vanillyl-azole-Schiff bases (IVASBs) have synthesized and their antitumor performances were assessed *in vitro* against MCF-7 cells and *in vivo* against Ehrlich solid tumor (EST). The high binding energy score of IVASB3-CDK1 (-3.43 kcal/mol) makes IVASB3 the most potent anti-breast cancer candidate (IC<sub>50</sub> 3.73 ± 0.2 µg/mL). Cell cycle analysis showed that IVASB<sub>3</sub> was significantly increased the percent of EST cells undergoing the sub G1 phase and decreased the percent of cells in the S phase. In addition, the administration of IVASB<sub>1</sub>, IVASB<sub>2</sub>, and IVASB<sub>3</sub> to tumorized mice caused a significant reduction in cyclin-dependent kinase-1 (CDK1) expression by 41.27%, 53.31%, and 78.57%, respectively. Moreover, concentrations of poly ADP-ribose polymerase (PARP) and vascular endothelial growth factor (VEGF) significantly decreased in the serum of tumorized mice which received IVASBs. Consequently, the antitumor effects of IVASBs could be attributed to their capacity to diminish CDK1, PAPR, and VEGF expressions.

© 2021 Elsevier B.V. All rights reserved.

## 1. Introduction

Cancer is one of the most serious human health problems and considered the second major reason for death all over the world [1,2]. Cancer is widely progressed in the modern era and is expected to hit ~25 million people in the next 20 years [3]. Breast cancer is the most frequent type of cancer among women worldwide; it is still a leading cause of global women's death. It accounts for about 450,000 deaths around the world yearly [4]. Current treatment strategies are based on surgical removal of the tumor or radiotherapy followed by chemotherapy [5]. Although chemotherapy and radiotherapy are broadly being used to treat numerous types of tumors, they suffer from many problems such as (i) non-selectivity and destructive side effects on normal cells; (ii) narrow-spectrum; and (iii) chemotherapeutic agent resistance [6]. Therefore, there is still an urgent need for the development of more safe and effective anticancer agents for wiping out this disease.

For the last few decades, an infinite number of researchers have demonstrated great interest in the nitrogen- and sulfur-containing heterocyclic compounds for the development of varieties of new biomolecules to enrich their therapeutic potential in pharmacological applications [7,8]. Amongst these compounds, 2-aminothiazole (AT) and its derivatives (Fig. S1, ESI†), which found in many natural products, always offer a class of promising bioactive scaffolds to design and develop diverse pharmacological agents with excellent biological activities [9]. In particular, Abafungin, Cefdinir, Famotidine, and Riluzole (Fig. S1, ESI†) are well-known marketing drugs bearing the 2-aminothiazole moiety [10]. Moreover, 2-aminothiazoles have proved to have various therapeutic potentials including antibacterial [11,12], antifungal [13], antiviral [14], anti-inflammatory [15], antioxidant [16], antidiabetic [17], anticonvulsant [18], and antitubercular [19]. In spite of the diverse biological impacts of 2-aminothiazole derivatives, 2-aminothiazole is still categorized as a promising scaffold for the construction of new potent anticancer agents due to their broad-spectrum antitumor activities through acting on different biological targets such as tubulin protein, HAT/HDAC enzymes, PI3K, Src/Abl, EGFR, BRAF, and SphK kinase [10,20]. Meanwhile, 1,3,4-thiadiazole ring is also considered a versatile scaffold for the development of multifunctional phar-

\* Corresponding author at: Chemistry Department, Faculty of Science, Suez University, Suez 43533, Egypt.

E-mail address: [reda.elshaarawy@suezuniv.edu.eg](mailto:reda.elshaarawy@suezuniv.edu.eg) (R.F.M. Elshaarawy).

macological agents [21]. Where, the mesoionic nature of this ring enables thiazole-based compounds to easily go through the cellular membrane and strongly interact with biological targets [22]. Furthermore, the anticancer potentials of thiazole derivatives are undeniable [22,23].

Notable, Schiff bases also have attracted great interest of many pharmaceutical researchers due to their biological performances in many fields [24] including anticancer efficacy [25].

Interestingly, the exceptional and amazing physicochemical properties of ionic liquids (ILs) makes them very attractive for many researchers to design numerous smart materials, rendering them inimitably suited for applications in many fields such as synthesis [26], electrochemistry [27], analytics [28], active pharmaceutical ingredients (API) [29], extraction [30], and so far. Recently, ionic liquid-supported Schiff bases were effectively used as chemical sensors [31,32] and to convert the toxic pollutants (primary amines and heavy metal ions) into pharmacological candidates [33,34].

There are a number of *in vivo* experimental models based on laboratory animals including the Ehrlich solid tumor (EST), derived from the mouse breast adenocarcinoma, which is an aggressive and fast growing carcinoma able to develop both in the ascetic or the solid form depending on whether inoculated intraperitoneally or subcutaneously, respectively [35]. It is a neoplasm of epithelial origin and can be used to study the mechanisms of carcinogenesis and evaluate the effect of new therapeutic approaches on tumors [36].

The cell cycle is composed of four functional phases (Fig. S2, ESI†) that lead to the duplication and division of cell: S phase involves DNA duplication; M phase (mitosis) where DNA and cellular components have divided into two daughter cells; G2 phase, where cells prepare for mitosis; G1 where cells prepare itself for other DNA and cellular divisions [37]. The transition from one phase to another is regularly occurred by the action of key regulatory proteins (Cyclin-dependent kinases (CDKs)) (Fig. S2, ESI†) [38]. Cyclin-dependent kinase 1 (CDK1) serves an important role in the control of the cell cycle by regulating the centrosome cycle, sponsoring G2-M transition, moderating G1 phase progression, and involved in the regulation of apoptosis, as well [39]. Noteworthy, CDK1 is overexpressed in several tumors and contributes to their development [40]. Therefore, studying the cell cycle through flow cytometric analysis could be very helpful in offering an insight concerning the mode of action for a new anticancer drug.

Herein, through our continuous efforts to explore new multifunctional bioactive ionic liquids-supported Schiff bases (ILSSBs) [41–43], three hybrid ionic vanillyl-azole-Schiff bases (IVASBs), (3-(thiazol-2-ylimino)methyl)vanillyl-2-methylimidazolium chloride (IVASB<sub>1</sub>), 2,5-Bis-(5-(2-methylimidazolium chloride)-3-methoxysalicylideneimino)-1,3,4-thiadiazole (IVASB<sub>2</sub>), and 2,5-Bis-(5-(2,4-lutidinium chloride)-3-methoxysalicylidene-imino)-1,3,4-thiadiazole (IVASB<sub>3</sub>), have been successfully fabricated. The effect of IVASBs against EST, induced experimentally in mice, was investigated in comparison to a reference chemotherapeutic drug, 5-fluorouracil, and examined their effect on CDK, PARP, and VEGF as well.

## 2. Materials and methods

### 2.1. Materials and instrumentation

Solvents and reagents coupled with their suppliers, methods used for the preparation of vanillyl ionic liquids (VILs) (2a,b) and 2,5-diaminothiadiazoole, and the instrumental techniques applied for the full characterization of the as-prepared ionic liquids were given in the online electronic supplementary information (ESI†).

### 2.2. Synthesis of IVASBs

In general, a solution of SMILs (5 mmol) in ethanol (25 mL) was added dropwise under vigorous stirring to a solution of 2-aminothiazole/ 2,5-diaminothiadiazoole (0.25/ 0.28 g, 5/ 2.5 mmol) in 10 mL of ethanol containing few drops of glacial acetic acid. The reaction mixture was further stirred under reflux temperature for 4–6 h (thin-layer chromatography (TLC) was used to monitor reaction progress). At the end of the reaction, the content was cooled to ambient temperature and the formed solids were collected by filtration, washed with cold ethanol (2 × 3 mL) followed by diethyl ether (3 × 5 mL), dried, and then recrystallized from ethanol to give the desired products.

3-(Thiazol-2-ylimino)methyl)vanillyl-2-methylimidazolium chloride (IVASB<sub>1</sub>): Obtained as yellowish-orange powder (96%). FTIR (KBr, cm<sup>-1</sup>): 3421 (vs, br), 3098 (m, br), 3061 (m, br), 1621 (s, sh), 1573 (w, br), 1509 (vs, sh), 1459, 1385 (w, b), 1283 (m, sh), 1149 (m, sh), 1065 (w, br), 745 (m, br). <sup>1</sup>H NMR (500 MHz, DMSO-*d*<sub>6</sub>) δ (ppm): 11.13 (s, 1H), 9.12 (s, 1H), 8.89 (s, 1H), 8.77 (s, br, 1H), 7.67–7.61 (m, 1H), 7.65–7.55 (m, 1H), 7.28 (s, 1H), 7.17 (d, *J* = 10.85 Hz, 1H), 7.10 (s, 1H), 5.25 (s, 2H), 3.86 (s, 3 H), 2.48 (s, 3H). <sup>13</sup>C NMR (125 MHz, DMSO-*d*<sub>6</sub>) δ (ppm): 161.95, 158.82, 157.09, 147.19, 144.65, 131.11, 125.71, 123.03, 121.28, 118.65, 106.38, 101.73, 55.88, 51.36, and 11.93. ESI-MS, *m/z*: 315.3 ([C<sub>15</sub>H<sub>15</sub>N<sub>4</sub>O<sub>2</sub>S]<sup>+</sup>, M - Cl<sup>-</sup>). Anal. Calcd. for C<sub>15</sub>H<sub>15</sub>ClN<sub>4</sub>O<sub>2</sub>S (*M* = 350.82): C, 51.36; H, 4.31; N, 15.97; S, 9.14%. Found: C, 51.33; H, 4.32; N, 15.94; S, 9.07%.

2,5-Bis-(5-(2-methylimidazolium chloride)-3-methoxysalicylideneimino)-1,3,4-thiadiazole (IVASB<sub>2</sub>): Obtained as orange powder (79%). FTIR (KBr, cm<sup>-1</sup>): 3429 (s, br), 2927 (m, br), 1629 (m, br), 1568 (m, sh), 1449 (m, br), 1284 (s, sh), 1201 (w, br), 1167 (w, sh), 1043 (m, br), 720 (w, br). <sup>1</sup>H NMR (500 MHz, DMSO-*d*<sub>6</sub>) δ (ppm): 11.12 (s, 2H), 11.09 (s, 1H), 10.83 (s, 1H), 10.12 (s, 1H), 9.97 (s, 1H), 8.07 (d, *J* = 1.83 Hz, 2H), 7.85–7.49 (m, 4H), 7.43 (d, *J* = 1.71 Hz, 2 H), 7.16–6.91 (m, 2H), 5.38 (s, 4H), 3.79 (s, 3H), 3.77 (s, 3H), 2.66 (s, 3H), 2.63 (s, 3H). <sup>13</sup>C NMR (125 MHz, DMSO-*d*<sub>6</sub>) δ (ppm): 164.93, 161.28, 158.19, 136.31, 128.65, 125.73, 123.31, 121.35, 118.51, 118.08, 57.58, 39.42 and 10.63. ESI-MS, *m/z*: 582.00 ([C<sub>26</sub>H<sub>26</sub>ClN<sub>8</sub>O<sub>4</sub>S]<sup>+</sup>, M - Cl<sup>-</sup>), 273.2 ([C<sub>26</sub>H<sub>26</sub>N<sub>8</sub>O<sub>4</sub>S]<sup>2+</sup>, M - 2Cl<sup>-</sup>). Anal. Calcd. for C<sub>26</sub>H<sub>26</sub>Cl<sub>2</sub>N<sub>8</sub>O<sub>4</sub>S (*M* = 617.51): C, 50.57; H, 4.24; N, 18.15; S, 5.19%. Found: C, 50.58; H, 4.26; N, 18.11; S, 5.16%.

2,5-Bis-(5-(2,4-lutidinium chloride)-3-methoxysalicylideneimino)-1,3,4-thiadiazole (IVASB<sub>3</sub>): Obtained as yellow powder (82%). FTIR (KBr, cm<sup>-1</sup>): 3423 (s, br), 2928 (w, br), 1632 (vs, sh), 1551 (w, br), 1449 (s, sh), 1273 (s, sh), 1209 (w, sh), 1155 (m, sh), 1039 (w, br), 710 (m, sh). <sup>1</sup>H NMR (500 MHz, DMSO-*d*<sub>6</sub>) δ (ppm): 11.13 (s, 2H), 10.28 (s, 1H), 10.03 (s, 1H), 8.79 (d, *J* = 4.3 Hz, 2H), 8.49 (s, 1H), 8.13–8.02 (m, 1H), 7.89 (d, *J* = 8.2 Hz, 2H), 7.75 (s, 1H), 7.46–7.35 (m, 1H), 7.26 (d, *J* = 6.1 Hz, 2H), 7.18 (dd, *J* = 11.9, 8.4 Hz, 2H), 5.31 (s, 4H), 3.87 (s, 6H), 3.78 (s, 6H), 2.76 (s, 6H). <sup>13</sup>C NMR (125 MHz, DMSO-*d*<sub>6</sub>) δ (ppm): 160.12, 155.89, 153.87, 147.11, 145.88, 133.15, 130.59, 128.90, 127.29, 126.31, 118.79, 117.81, 57.59, 22.13, and 21.21. ESI-MS, *m/z*: 646.10 ([C<sub>33</sub>H<sub>34</sub>ClN<sub>6</sub>O<sub>4</sub>S]<sup>+</sup>, M - Cl<sup>-</sup>), 305.30 ([C<sub>33</sub>H<sub>34</sub>N<sub>6</sub>O<sub>4</sub>S]<sup>2+</sup>, M - 2Cl<sup>-</sup>). Anal. Calcd. for C<sub>34</sub>H<sub>36</sub>Cl<sub>2</sub>N<sub>6</sub>O<sub>4</sub>S (*M* = 695.66): C, 58.70; H, 5.22; N, 12.08; S, 4.61%. Found: C, 58.64; H, 5.26; N, 12.91; S, 4.42%.

### 2.3. Docking study

AutoDock4 was employed for docking the tested compounds (IVASBs) in the binding site of CDK1. The X-ray crystal structure of CDK1 was obtained from RCSB Protein Data Bank (PDB ID: 4YC6) with a 2.6 Å resolution. The protein targets were prepared for molecular docking simulation by removing water molecules and bound ligands. IVASBs were built and modeled using the MDL ISIS Draw 2.5 software.

## 2.4. In vitro cytotoxicity experiment

The *in vitro* cytotoxic impact of ionic vanillyl azole Schiff bases (IVASBs) on human breast carcinoma cell lines (MCF-7) was evaluated according to the protocol adapted by the regional center for Mycology and Biotechnology, Al-Azhar University, Egypt as described in our previous work [44]. 5-Fluorouracil (5-FU) was used as a reference drug. The cell viability and IC<sub>50</sub> values were used as cytotoxicity markers for the tested compounds.

## 2.5. In vivo study

### 2.5.1. Determination of median lethal dose (LD<sub>50</sub>)

The median lethal dose (LD<sub>50</sub>) of the test compounds was determined according to the method described by Reed and Muench [45]. Briefly, the method involves the intraperitoneal injection of single dose of different dilutions for each test compound separately to various groups, which has ten mice each. After that the injected mice were observed for behavior and mortality for 24 h. The number of survival and dead mice was recorded and the percent of mortality was calculated for each group and LD<sub>50</sub> was calculated using the following formula;

$\text{Log LD}_{50} = \log \text{LD next below } 50\% + [\log \text{ increasing factor} \times \text{Proportional distance}]$  where,  $\text{proportional distance} = [50 - \text{mortality at dilution next below}] / [\text{mortality next above} - \text{mortality next below}]$ . LD<sub>50</sub> values of IVSB<sub>1</sub>, IVSB<sub>2</sub> and IVSB<sub>3</sub> were recorded at 3.31 µg/Kg b.w., 55 and 450 mg/Kg b.w., respectively.

### 2.5.2. Experimental animals, ethics and cancer cell lines

Swiss albino mice samples (20–25 g) were housed in plastic cages under standard laboratory conditions (25 ± 2 °C; 70–80 humidity; 12 h light/darkness cycle) with standard pellet diet and water *ad libitum*. The animals were handled in accordance with current guidelines for the care of laboratory animals and ethical guidelines for the investigation of experimental pain in conscious animals. The first inoculum of Ehrlich ascites carcinoma (EAC) and MCF-7 cell lines was purchased from the national cancer institute (Cairo, Egypt). EAC cells were propagated in the peritoneal cavity of mice through serial intraperitoneally (IP) transplantation of 10<sup>6</sup> cells (0.2 ml of PBS/animal) and transferred every 7 days to normal animals.

### 2.5.3. Ehrlich solid tumor (EST) model

A total of 90 male albino mice were randomly divided into six groups (15 mice/ group). Group I was kept as control while the solid tumor was induced in the other five groups. On the day of induction, Ehrlich cells were collected from the ascitic fluid of a female Swiss albino mouse bearing an 8-day-old ascetic tumor obtained from the National Cancer Institute (Cairo, Egypt). The ascitic fluid was diluted with normal saline (1: 10 v/v). Solid tumors were induced by intramuscular inoculation of 0.2 mL of ascitic fluid, containing approximately 2.5 × 10<sup>6</sup> EAC cells, in the right thigh of the hind limb of each mouse [46]. After 2 weeks of tumor inoculation mice were treated intraperitoneally with test compounds (IVASB<sub>1</sub>, IVASB<sub>2</sub> and IVASB<sub>3</sub>) or 5-fluorouracil (5-FU) every other day according to the following scheme:

- Group I: normal mice saline-control group (normal control): fifteen normal mice have injected IP with 0.2 mL physiological saline (0.9 g/dL) every other day for 13 days.
- Group II: fifteen tumorized mice control group (Ehrlich control).
- Group III: tumorized mice L1-treated group (EST + IVASB<sub>1</sub>): fifteen tumorized mice treated with L1 (1/10 LD<sub>50</sub>; 0.331 µg/Kg) every other day for 13 days.
- Group IV: tumorized mice treated with L2-treated group (EST + IVASB<sub>2</sub>): fifteen tumorized mice treated with L2 (1/10 LD<sub>50</sub>; 5.5 mg/Kg) every other day for 13 days.

- Group V: tumorized mice L3-treated group (EST + IVASB<sub>3</sub>): fifteen tumorized mice treated with L3 (1/10 LD<sub>50</sub>; 45 mg/Kg) every other day for 13 days.
- Group VI: tumorized mice 5-fluorouracil (5-FU)-treated group (EST + 5-FU): fifteen tumorized mice treated with 5-FU (20 mg/Kg) every other day for 13 days.

The volume of the solid tumor was evaluated using Vernier caliper (after shaving the tumor-bearing thigh of each animal) and was calculated using the formula of  $A \times B \times 0.5$ , where A and B are the longest and the shortest diameter of tumor, respectively [47]. Then, the tumor mass was removed, weighed, tabulated, and preserved in buffered formalin and stored at –80 °C until further use and processed for flow cytometry investigations of the tumor marker cyclin-dependent kinase 1 (CDK1) and cell cycle analysis.

## 2.6. Hematological parameters

At the end of the *in vivo* experiment, the animals were sacrificed under slight ether anesthesia by cervical dislocation and blood samples were taken in tubes containing EDTA for determination of hematological parameters. Hemoglobin (HGB), count of white blood cells (WBCs), and red blood cells (RBCs) were analyzed using standard automated procedures.

## 2.7. Biochemical parameters

Blood samples were taken in tubes without anticoagulant (for serum biochemical analysis in accordance with the method of Frankenberg [48]). Sera were separated and stored in aliquots at –80 °C until using for analysis of biochemical parameters of aspartate transaminase (AST), alanine transaminase (ALT), the concentration of albumin (Alb), total bilirubin (T bil), urea and creatinine, and ELISA technique of Poly-ADP-ribose polymerase (PARP) and vascular endothelial growth factor (VEGF).

### 2.7.1. Determination of poly ADP-ribose polymerase (PARP)

The concentration of PARP in the serum of mice was determined using a commercial ELISA kit applying the quantitative sandwich enzyme immunoassay technique. The microtiter plate has been pre-coated with a monoclonal antibody specific for PARP. Standards or samples were added to the microtiter plate wells and PARP will bind to the antibody pre-coated wells. In order to quantitatively determine the amount of PARP present in the sample, a standardized preparation of horseradish peroxidase (HRP)-conjugated polyclonal antibody, specific for PARP is added to each well to “sandwich” the PARP immobilized on the plate. Then the wells are thoroughly washed to remove all unbound components. Next, substrate solutions are added to each well. The enzyme (HRP) and substrate are allowed to react over a short incubation period. Only those wells that contain PARP and enzyme-conjugated antibody will exhibit a change in color. A standard curve is plotted relating the intensity of the color (OD) to the concentration of standards. The PARP concentration in each sample is interpolated from this standard curve. The Optical Density (OD) was determined at 450 nm using a microplate reader.

### 2.7.2. Determination of vascular endothelial growth factor (VEGF)

The concentration of VEGF in serum of mice was determined using ELISA commercial Kit (Invitrogen, USA) and the procedure was followed according to the manufacturer's instructions. Briefly, a mouse monoclonal antibody specific for rat VEGF is coated on a 96-well plate. Standards and test samples are added to the wells and VEGF present in a sample is bound by the immobilized antibody. A biotinylated polyclonal antibody from goat specific for VEGF is added subsequently. After washing away the unbound

biotinylated antibody with PBS or TBS buffer, the avidin-Biotin-Peroxidase complex is added to the wells. The wells were again washed with PBS or TBS buffer to remove the unbound conjugates. HRP substrate TMB is used to visualize the HRP enzymatic reaction. TMB is catalyzed by HRP to produce a blue product that changes into yellow after adding the acidic solution. The density of yellow color is proportional to the quantity of VEGF captured onto the plate. The Optical Density (OD) was determined at 450 nm using a microplate reader.

### 2.8. Flow-cytometric analysis

The flow-cytometric analysis was performed in the global center for scientific research, Mansoura, Egypt using FACS (Flow activated cell sorter) Caliber Flow Cytometer (Becton Dickinson, Sunnyvale, CA, USA) equipped with a compact air-cooled low power 15 mW argon ion laser beam (488 nm). Data analysis was conducted using DNA analysis program MODFIT (verity software house, Inc. Po Box 247, Topsham, ME 04,086 USA, version: 2.0 powers Mac with 131,072 KB Registration No: 42,000,960,827 Date made: 16-Sep, 1996). This software measured cell cycle analysis, which was calculated the coefficient of variation (CV) around the  $G_0/G_1$  peak and the percentage of cells in each phase ( $G_0/G_1$ , S, and  $G_2/M$ ) of the DNA cell cycle for each sample. The analysis of apoptotic cell death was performed by measuring DNA content.

#### 2.8.1. Cell cycle analysis

After washing the cells with PBS, EAC cells were fixed by ice-cold absolute alcohol and then centrifuged and excessive alcohol was removed. The cells were re-suspended in citrate buffer and then were stained with PI. The DNA content was measured using an Accuri C6 flow cytometer (Becton Dickinson, Sunnyvale, CA, USA).

#### 2.8.2. Flowcytometric evaluation of cyclin dependent-kinase 1(CDK1) in Ehrlich cells

To prepare the cells, they were fixed in a solution of 1% formaldehyde for 15 min at 4 °C, then washed with phosphate-buffered saline (PBS) containing 1% fetal calf serum (FCS, Sigma, St. Lois, USA), after that the cells were fixed in 80% ethanol with vortexing to prevent the aggregation of cells. The fixed cells were kept in 80% ethanol at -20 °C until use. Before the assay, the cells were washed with wash buffer (WB) at 400 g for 10 min, so as to remove the ethanol, and then incubated with WB containing Triton X-100 for 5 min at 4 °C in order to perforate the cells.

The expression of CDK1 was performed using the FITC conjugates of the antibodies specific to CDK1 (Pharmlingen, USA). The percent of cells expressed CDK1 was assessed using fluorescence threshold by FACS Caliber Flow Cytometer (Becton Dickinson, Sunnyvale, CA, USA).

### 2.9. Statistical analysis

All the data were expressed as a mean  $\pm$  standard error of the mean (SEM) to compare between EAC control and treated groups. The statistical significance was evaluated by one-way analysis of variance using SPSS, 16.0 software (SPSS Corp, Chicago, IL), and individual comparisons were done by Duncan's multiple range test. Values were considered statistically significant when  $p < 0.05$ , high statistically significant when  $p < 0.01$  and very high statistically significant when  $p < 0.001$ .

## 3. Results and discussion

### 3.1. Chemistry

Different chemical processes including chloromethylation, quaternization, heterocyclization, Schiff-base condensation were used in our protocol to synthesize the target compounds (see **Scheme 1**). Initially, chloromethylation of salicylaldehyde was performed using a mixture of paraformaldehyde and hydrochloric acid in presence of  $ZnCl_2$  to yield chloromethylsalicylaldehyde (**1**) that used as alkylating agent for quaternization of 2-methylimidazole (2-Melm), 2,4-dimethylpyridine (2,4-lutidine, 2,4-Lut) to fabricate salicylaldehyde ionic liquids (SILs, **2a,b**).

On the other hand, 2,5-diamino-1,3,4-thiadiazole was obtained by the heterocyclization of bis-thiourea by the action of hydrogen peroxide. Eventually, the Schiff base condensation of SILs (**2a,b**) with 2-AT or diaminothiadiazole produce the desired ionic vanillyl azole Schiff bases (IVASBs) (**Scheme 1**). These ionic Schiff bases were obtained with high to excellent yields and their structures were elucidated based on the elemental and spectral (FTIR,  $^1H$  NMR,  $^{13}C$  NMR, ESI-MS) analyses.

### 3.2. Structural characterizations of IVASBs

#### 3.2.1. Elemental analysis and mass spectrometry

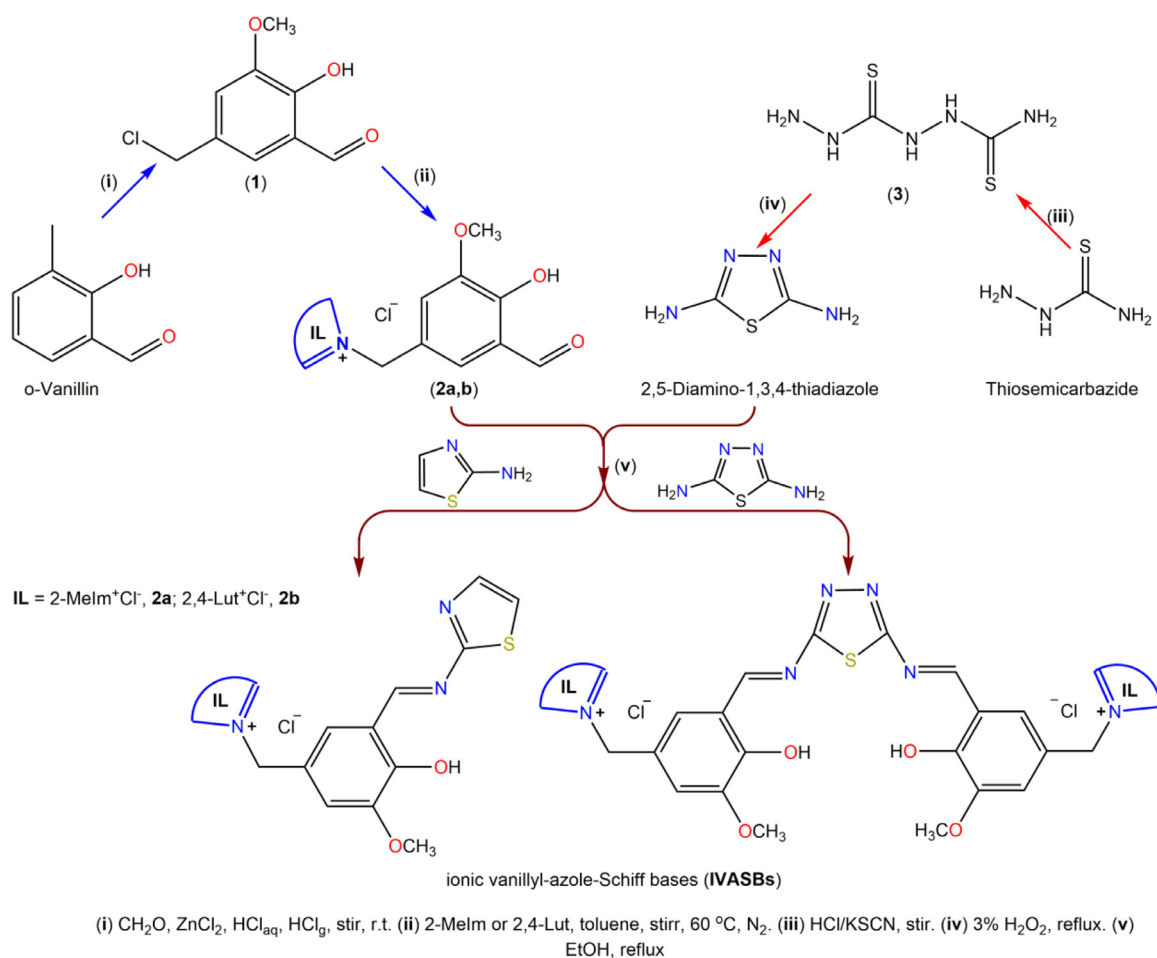
The new ionic Schiff bases exhibited acceptable microanalytical data that in full consistent with the proposed structural formula for them (see the Experimental part). Moreover, the positive-mode electrospray ionization mass spectrometry (ESI-MS) of these Schiff bases exhibited main peaks at  $m/z$  315.3, 582.0, and 646.1 assigned to the singly-charged cation  $[M - Cl^-]$  of IVASB<sub>1</sub>, IVASB<sub>2</sub> and IVASB<sub>3</sub>, respectively. In addition, IVASB<sub>2</sub> and IVASB<sub>3</sub> display another peak at  $m/z$  273.2 and 305.3, respectively, assigned to the doubly-charged cation  $[M - 2Cl^-]$ . These findings offer further support for the authenticity of the suggested structures.

#### 3.2.2. FTIR

Usually, the IR analysis provides a shred of preliminary evidence for the success of the preparation of a new compound [49]. For this purpose, the comprehensive comparison between the FTIR spectra of SIL<sub>1</sub> (**2a**), 2-AT, and, IVASB<sub>1</sub> (**Fig. 1A**) revealed the disappearance of the stretching vibration bands distinctive for the amine group of AT (centered at 3412 and 3295  $cm^{-1}$  in the 2-AT spectrum) and the aldehydic carbonyl group of SIL<sub>1</sub> (centered at 1674  $cm^{-1}$  in the SIL<sub>1</sub> spectrum) in the spectrum of IVASB<sub>1</sub>. Besides, new stretches have emerged in the IVASB<sub>1</sub> spectrum at 3411, 1614, and 1279  $cm^{-1}$  characteristic for the phenolic O-H, azomethine, and Aryl-O groups, respectively, of salicylidene Schiff base segment. Furthermore, the main peaks distinctive for the imidazolium moiety can be noticed 1450 and 852  $cm^{-1}$  in the IVASB<sub>1</sub> spectrum [50].

In the same context, comparison of the spectra of ionic bis-(salicylideneimino)-thiadiazoles (IVASB<sub>2</sub> and IVASB<sub>3</sub>) with those of SIL<sub>1,2</sub> (**2a,b**), and 2,5-diamino-1,3,4-thiadiazole (DAT) (**Fig. 1B**) evident missing of the stretches of amine group of DAT (3490 and 3420  $cm^{-1}$  in DAT spectrum) and the aldehydic carbonyl groups of SIL<sub>1,2</sub> (1680  $\pm$  7  $cm^{-1}$  in the SIL<sub>1,2</sub> spectra) in the spectrum of IVASB<sub>2,3</sub>. Instead, a new set of vibration bands have emerged in the spectra IVASB<sub>2,3</sub> round 3425, 1610, 1289, 1423, and 845  $cm^{-1}$  assignable for the vibration of phenolic O-H, azomethine (H-C=N), Aryl-O groups, and imidazolium or pyridinium ring, respectively, of ionic salicylidene Schiff base segments [51].

These findings confirm the successful formation of IVASBs by Schiff base condensation of the amine group(s) of 2-AT or DAT with carbonyl group of SILs.



**Scheme 1.** Stepwise protocol used for preparation of salicylaldehyde ionic liquids (SILs, **2a,b**), 2,5-diaminothiadiazole, and ionic vanillyl azole Schiff bases (IVASBs).

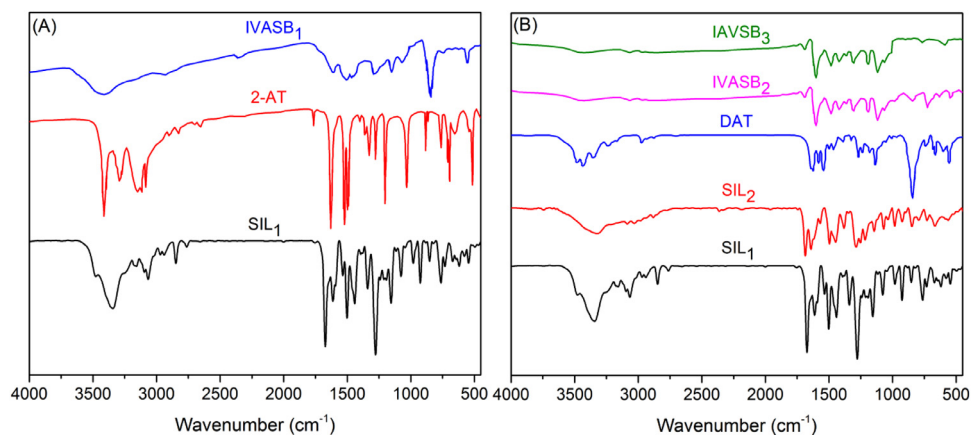


**Fig. 1.** Collective FTIR spectra of 2-AT, DAT, SILs, and ionic vanillyl azole Schiff bases (IVASBs) for comparison of their respective spectral signatures, particularly, the azomethine (H-C=N) and aryl-O vibration bands.

### 3.2.3. NMR spectroscopy

The common spectral features of <sup>1</sup>H NMR spectra for new Schiff bases (IVASBs) are the disappearance of the low-field singlets distinctive for the aldehydic and amine protons of native SILs (~10.30 ppm) and AT or DAT (~6.20 ppm), respectively. Instead, new singlet peaks have observed around 8.48 ppm assigned to the azomethinic proton (H-C=N), confirming the success of Schiff base condensation between the amine group(s) of 2-AT or DAT and aldehydic group of SILs to form IVASBs. Furthermore, compared to the spectrum of DAT, three new sets signals have emerged in the

spectrum of IVASB<sub>2</sub> (Fig. 2) at the chemical shift ranges 11.13 – 10.0, 7.62 – 6.91, and 5.51 – 2.95 ppm assignable to the resonance of imidazolium N-H, phenolic O-H, aromatic Ar-H, methylene CH<sub>2</sub>, and methyl CH<sub>3</sub> protons of the imidazolium salicylidene fragment [52].

<sup>13</sup>C NMR spectra of IVASBs offers additional evidences emphasizing their successful preparation as evident from notice of two down-field peaks around δ 161 ppm and 147 ppm corresponding to carbon atoms bonded to azomethine nitrogen and phenolic oxygen, respectively.

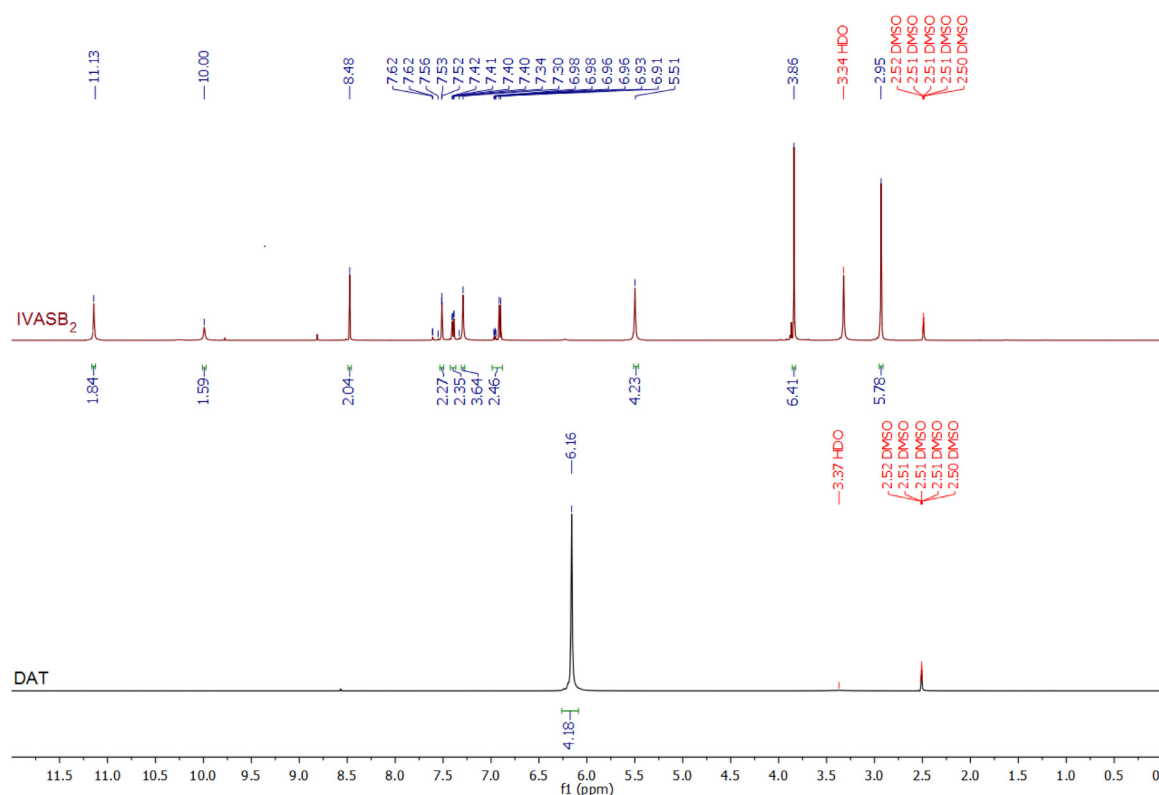


Fig. 2.  $^1\text{H}$  NMR spectra of 2,5-diamino-1,3,4-thiadiazole (DAT) and IVASB<sub>2</sub> in  $d_6$ -DMSO at 300 MHz.

### 3.3. Docking study

CDKs play a vital role in the regulation of cell cycle and proliferation and their functions qualify them to be convenient targets for anticancer agents [53,54]. CDK1 in combination with cyclin B promotes entry into mitosis and regulates several processes of mitotic progression [53,55]. An increase in the expression of CDK1 was observed in human cancer [56], therefore CDK1 inhibition represents a great benefit in cancer treatment. The molecular docking study was applied to investigate the binding modes and affinities of the newly synthesized Schiff bases (IVASBs) with the active sites of CDK1. The calculated docking scores for IVASBs and the interacted amino acid residues of CDK1 with new ionic Schiff bases were tabulated in Table S1 (ESI†). As evident in Table S1, all Schiff bases exhibit good binding affinities toward CDK1 with binding energy (BE) values ranged from  $-2.30$  to  $-3.52$  kcal/mol, indicating that the CDK1 inhibition is a reasonable mechanism for interpreting the anticancer effect of these compounds.

As shown in Figs. 3 (A, D) and S3 (ESI†), IVASB<sub>1</sub> exhibited an interesting binding model with CDK1 where it has interacted through two types of bindings: (i) Three H-bonds (HB), between nitrogen atoms of azomethine and thiazole moieties hydroxyl groups of amino acid residues (AAR) (Thr25, Arg47, and Tyr26). (ii) One hydrophobic binding (HPOB), between the phenyl ring and carbon chain of IVASB<sub>1</sub> and Glu32, respectively. Also, IVASB<sub>2</sub> has bound to CDK1 by H-bonding and HPOB but with different binding models as evident in Figs. 3 (B, E) and S4 (ESI†) with lower BE values as compared to IVASB<sub>1</sub>. Interestingly, the IVASB<sub>3</sub>-CDK1 binding involves three types of interactions Figs. 3 (C, F) and S5 (ESI†); HB, between N-atom of DAT and OH group of Gly24;  $\pi$ -stacking, between phenyl rings of DAT and Tyr26; HPOB, between the phenyl ring and carbon chain of IVASB<sub>3</sub> and Glu32, Thr25, Lys138, respectively. In addition to the wonderful IVASB<sub>1</sub>-CDK1 and IVASB<sub>3</sub>-CDK1 binding models, the binding energy scores of

IVASB<sub>1</sub> ( $-3.52$  kcal/mol) and IVASB<sub>3</sub> ( $-3.43$  kcal/mol) makes them the most potent anti-breast cancer candidates.

### 3.4. Cytotoxicity experiment

The MTT assay was applied to *in vitro* assess the cytotoxic effects of new ionic Schiff bases (IVASBs) toward human breast carcinoma cell lines (MCF-7) in comparison to a clinical drug 5-Fluorouracil (5-Fu). The MCF-7 cell viability and IC<sub>50</sub> values (Fig. 4) were used as biomarkers for cytotoxic performance. In general, the ionic liquids-supported Schiff bases (IVASB<sub>1</sub> and IVASB<sub>3</sub>) are more cytotoxic than 5-Fu, whereas, IVASB<sub>2</sub> is less than the clinical drug as revealed from the survival MCF-7 cells after each treatment (Fig. 4A). Just to name a few, the surviving MCF-7 cells were found to be 42.19, 83.53, 26.96, and 46.53 remediation of these cells with 16.60  $\mu\text{g}/\text{mL}$  of IVASB<sub>1</sub>, IVASB<sub>2</sub>, IVASB<sub>3</sub>, and 5-Fu, respectively. Furthermore, the IC<sub>50</sub> values of IVASB<sub>1</sub>, IVASB<sub>2</sub>, IVASB<sub>3</sub>, and 5-Fu were  $13.5 \pm 1.14$ ,  $102 \pm 6.3$ ,  $3.73 \pm 0.2$ , and  $28.12 \pm 2.25$   $\mu\text{g}/\text{mL}$ , respectively (Fig. 4B). According to our results, IVASB<sub>1</sub> and IVASB<sub>3</sub> are the most cytotoxic against MCF-7 human breast cancer cell lines and could offer promising anti-breast cancer candidates. Our findings agreed with the molecular docking results.

### 3.5. Influence of tested compounds on hematology of Ehrlich-tumorized mice

The data in Table 1 showed that treatment with thiazole resulted in significant EAC-induced alteration of hematological parameters compared to untreated Ehrlich-tumorized mice. White blood cells (WBCs) level was significantly reduced by the administration of IVASB<sub>1</sub>, IVASB<sub>2</sub>, and IVASB<sub>3</sub> ( $P \leq 0.001$ ,  $P \leq 0.01$ , and  $P \leq 0.01$ , respectively) compared to normal control group. Red blood cells count (RBCs) was increased in IVASB<sub>1</sub>-, IVASB<sub>2</sub>-, and IVASB<sub>3</sub>-treated mice by (8.7, 12.3, and 20.5%, respectively) com-

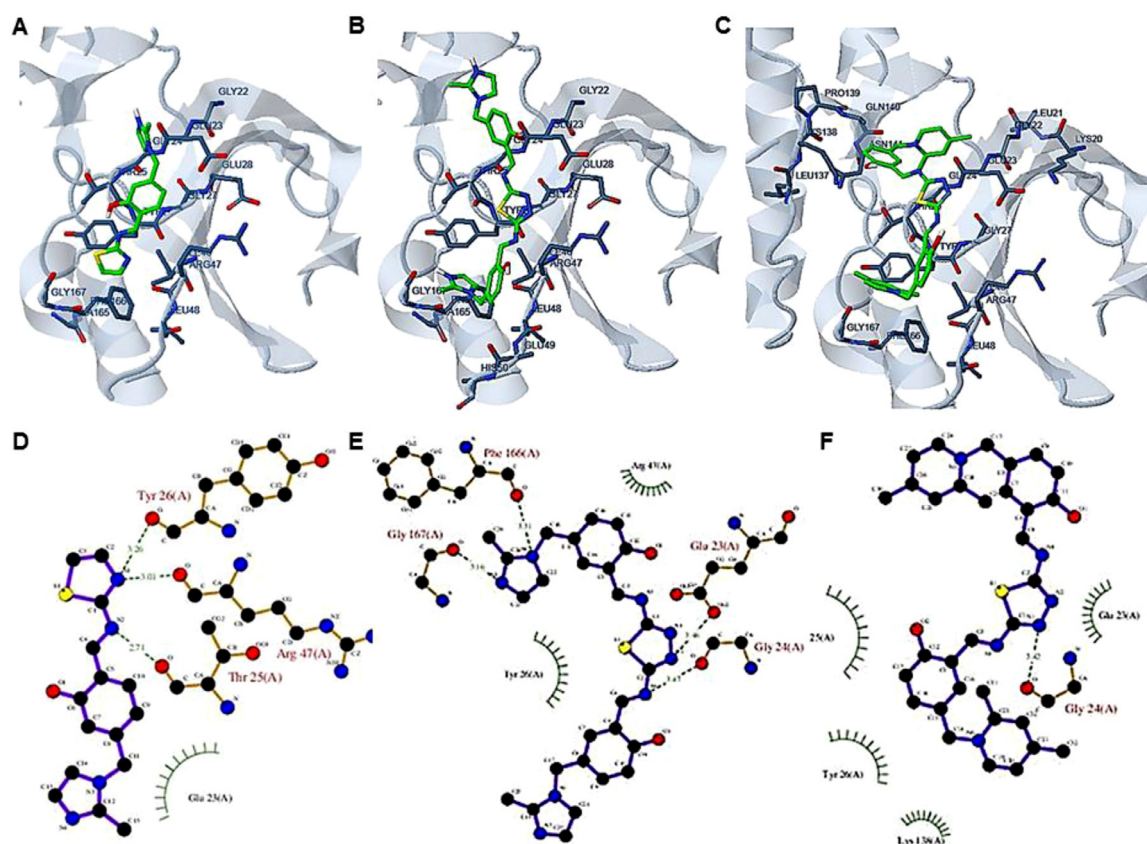


**Fig. 3.** (A–C) 2D molecular docking modeling of IVASB<sub>1</sub>, IVASB<sub>2</sub>, IVASB<sub>3</sub> (green stick molecule) with amino acid residues (AAR) of CDK1; showing hydrogen bonding (HB) (dotted lines), hydrophobic binding (HPOB), and  $\pi$ -stacking interactions (curved lines). (D,E) 3D model for the electrostatic map and interaction of IVASB<sub>1</sub>, IVASB<sub>2</sub>, and IVASB<sub>3</sub> with the CDK1 binding sites (For interpretation of the references to color in this figure legend, the reader is referred to the web version of this article.).

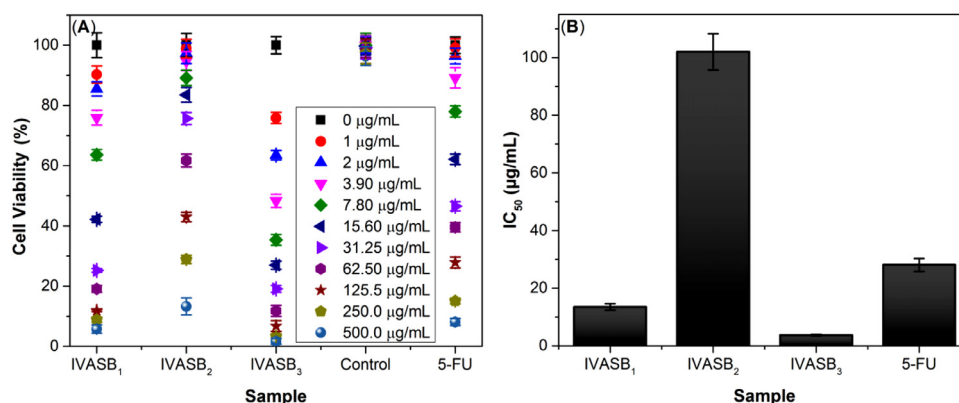


**Fig. 4.** (A) The cytotoxicity performance of new ionic Schiff bases (IVASBs) toward human breast carcinoma cell lines (MCF-7) in comparison to a clinical drug 5-Fluorouracil (5-Fu). (B) The IC<sub>50</sub> values of the tested compounds against MCF-7.

**Table 1**  
Effect of the tested compounds on hematological parameters †.

Parameter	Normal control M±SE	EAC control M±SE	EAC + SB <sub>1</sub> M±SE	EAC + SB <sub>2</sub> M±SE	EAC + SB <sub>3</sub> M±SE	EAC + 5-Fu M±SE
WBCs	10.3***±0.2	13.2 ± 0.38	7.73***±0.16	11.12**±0.11	11.21**±0.2	11.38**±0.5
RBCs	8.78**±0.15	7.6 ± 0.2	8.33*±0.03	8.67**±0.3	9.56***±0.02	8.64**±0.2
HGB	11.8***±0.2	8.6 ± 0.4	9.65*±0.2	12.8***±0.3	12.8***±0.2	9.9*±0.2
HCT	40.3***±0.4	27.9 ± 1.9	35.1**±0.7	46.3***±0.8	43.9***±0.6	35.7**±1.04
MCV	46.9**±0.9	42.7 ± 0.7	46.9**±0.7	50***±0.7	45.9*±0.8	52.2***±0.7
MCH	14.9**±0.3	13.2 ± 0.5	16.2***±0.2	15.8**±0.2	14.6*±0.3	15.8**±0.4
MHC	32.02***±0.3	27.5 ± 0.7	29.3*±0.3	31.7***±0.5	32.6***±0.9	33***±0.3
PLT	474**±22	381±22.4	541.2***±1.07	473.1**±1.5	324.6*±5.8	451.8*±19

† Values are represented as mean ±SE (n = 6), Where \* = Significant difference between test groups and Ehrlich control group, \*P ≤ 0.05, \*\*P ≤ 0.01, \*\*\*P ≤ 0.001. RBCs: red blood cell count; HGB: hemoglobin; HCT: hematocrit; MCV: mean corpuscular volume; PLT: platelet count; WBC: white blood cell count. SB<sub>1</sub> = IVASB<sub>1</sub>, SB<sub>2</sub> = IVASB<sub>2</sub>, and SB<sub>3</sub> = IVASB<sub>3</sub>.

**Table 2**  
The effect of the tested compounds on biochemical parameters †.

Groups	ALT (U/L)	AST (U/L)	Albumin (g/L)	TBil (mg/dL)	Urea (mg/dL)	Creatinine (mg/dL)
<b>EAC control</b>	80.61 ± 1.34	267.25 ± 3.89	2.14 ± 0.005	0.56±0.012	40.5 ± 0.76	0.59 ± 0.014
<b>EAC + SB<sub>1</sub></b>	47.86***±3.69	185.15***±2.73	2.396***±0.004	0.478**±0.015	36.5**±0.43	0.48**± 0.03
<b>EAC + SB<sub>2</sub></b>	59.32***±1.88	170.25***±2.54	2.37***±0.023	0.50 ± 0.03	35.16*±1.92	0.45***±0.016
<b>EAC + SB<sub>3</sub></b>	59.93***±1.02	154.05***±2.12	2.34***±0.027	0.503**±0.11	29.33***±0.88	0.37***±0.008
<b>EAC +5-FU</b>	60.84***±0.199	149.91***±4.42	2.301***±0.007	0.49*±0.02	35***±0.816	0.53*±0.025
<b>Control</b>	56.98***±1.68	186.23***±4.19	2.46***±0.012	0.44***±0.017	29.33***±0.88	0.35***±0.009

† Values are represented as mean±SE (n = 6), Where \* = Significant difference between Test groups and EAC control group, \*P ≤ 0.05, \*\*P ≤ 0.01 and \*\*\*P ≤ 0.001.

**Table 3**  
The effect of tested compounds on the cell cycle of Ehrlich cells†.

Phases	EAC control M±SE	EAC + SB <sub>1</sub> M±SE	EAC + SB <sub>2</sub> M±SE	EAC + SB <sub>3</sub> M±SE	EAC +5-FU M±SE
Sub G1	8.5 ± 1.4	70.5***±1.3	41.8***±1.2	86.03***±2.7	37.2***±2.2
G0/1	46.9 ± 0.8	13.2***±1.2	40.3*±1.4	10.1***±1.4	38.7*±1.9
S	34.8 ± 0.7	11.6**±1.8	15.1***±0.1	0.5***±0.3	21.03*±3.9
G2/M	5.1 ± 0.6	1.9**±0.3	6.2 ± 0.5	0.03***±0.03	5.5 ± 1.1

† Values are represented as mean ±SE (n = 6), Where \* = Significant difference between test groups and Ehrlich control group, \*P ≤ 0.05.

\*\* P ≤ 0.01.

\*\*\* P ≤ 0.001.

pared to Ehrlich control group, while hemoglobin (HGB) concentration was increased by (10.8, 32.8, and 32.8%, respectively) as compared to Ehrlich control group. Similarly, mean corpuscular volume (MCV) of red blood cells (RBCs) was significantly increased by the administration of IVASB<sub>1</sub> (8.9%), IVASB<sub>2</sub> (14.6%), and IVASB<sub>3</sub> (6.9%) compared to untreated Ehrlich control group. Only IVASB<sub>1</sub> and IVASB<sub>2</sub> can be induced significant elevation of platelet count (PLT) by (29.6% and 19.4%, respectively) as compared to untreated Ehrlich control group.

### 3.6. Effect of tested compounds on biochemical parameters of Ehrlich-tumorized mice

The data in **Table 2** showed that treatment with IVASBs caused significant Ehrlich-induced alteration of biochemical parameters compared to untreated Ehrlich control group. Results of the present study demonstrated that the liver activities of AST and ALT were increased in Ehrlich-tumorized mice when compared to normal control group. It was found that Ehrlich led to some liver dysfunction. The level of liver enzymes increased in serum of Ehrlich-tumorized mice indicating general toxicity found that Ehrlich mice exhibited raised activities of liver enzymes such as AST, ALT, due to hepatocellular damages. There was a significant decrease in serum ALT and AST of Ehrlich tumorized mice received compounds (IVASBs) (P ≤ 0.001 at all).

### 3.7. Flowcytometric analysis of Ehrlich solid tumor cell cycle phase distribution

One of the most important strategies for cancer chemotherapy to give an insight regarding the performance and mode of action for a new chemotherapeutic agent is the flowcytometric analysis. The cell cycle analysis of control and different treated mice groups were performed and the obtained results were collected in **Fig. 5** and **Table 3**. Noteworthy, treating of tumorized mice with IVASB<sub>3</sub> has significantly reduced the percent of cells in the G1 phase by 46.9% (4.64-times lower than that Ehrlich control group (10.1%)) (P ≤ 0.001). Furthermore, the percent of cells undergoing apoptosis in the tumorized mice, IVASB<sub>3</sub>-remediated, has increased by ~10-fold compared to the control group (P ≤ 0.001). In addition, the compound IVASB<sub>3</sub> significantly reduced the percent of cells in S phase by 69.6-fold compared to control group (P ≤ 0.001)

which confirmed that IVASB<sub>3</sub> arrested Ehrlich cells at G0/G1 check point. In the same way, the percent of cells undergoing apoptosis in Ehrlich-tumorized mice treated with compound IVASB<sub>2</sub> increased by 4.92-fold compared to control group (P ≤ 0.001) and the percent of cells in S phase significantly decreased by 2.30-fold compared to control group (P ≤ 0.001). Likewise, The administration of the compound IVASB<sub>1</sub> to tumorized mice led to a significant increase 8.29-fold in the percent of cells undergoing apoptosis compared to control group (P ≤ 0.001) and a significant decrease 3-fold in the percent of cells in S phase compared to tumor control group (P ≤ 0.01). Moreover, It was observed that the administration of IVASB<sub>1</sub> and IVASB<sub>3</sub> significantly decreases the percent of cells undergoing mitosis by 2.68 and 170-fold (P ≤ 0.01), respectively compared to Ehrlich control.

Based on the analysis of cell cycle by flowcytometry in the present study, all three test compounds increased the percentage of cells in sub G1 phase which indicates that these compounds exert their anticancer effect by inducing apoptosis. Previous report revealed that *p*-chlorophenethylamino and *p*-methoxyphenethylamino thiazole derivatives induced apoptosis in human U-937 leukemia cells in a time and concentration dependent manner [57]. In addition, the cell cycle analysis confirmed the G2/M-phase arrest and induction of apoptosis by thiazole derivatives in HeLa cells [58].

### 3.8. Effect of tested compounds on the expression of CDK-1 in Ehrlich cells

As shown in **Fig. 6**, the expression of CDK1 in Ehrlich cells collected from mice which received the compound IVASB<sub>1</sub> significantly decreased by 41.27% when compared to tumor control group (P ≤ 0.001) and the administration of compound IVASB<sub>2</sub> led to a decrease in the expression of CDK1 by 53.31% compared to Ehrlich control group (P ≤ 0.001), while the compound IVASB<sub>3</sub> was the most effective one causing a reduction of CDK1 expression by 78.57% compared to tumor control group (P ≤ 0.001).

Based on flow-cytometric analysis in our study, all three tested compounds were able to inhibit the expression of CDK1 by the percent of change ranging from 41.27% to 78.57% when compared to tumor control group and the most potent inhibitory effect was observed at IVASB<sub>3</sub>. Moreover, IVASB<sub>1</sub> and IVASB<sub>3</sub> caused cell cycle

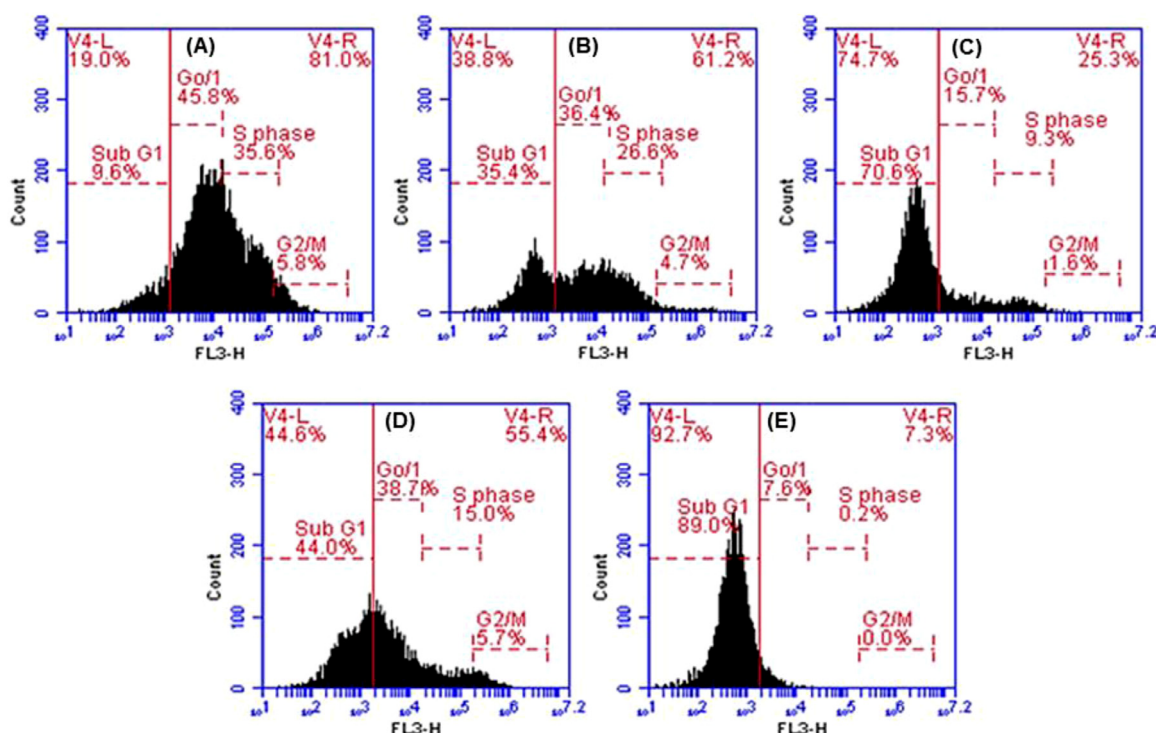


Fig. 5. Flow cytometric histogram showing; (A) Ehrlich control and the effect of (B) 5-Fu, (C) IVASB1, (D) IVASB2, and (E) IVASB3 on the cell cycle in Ehrlich tumorized mice.

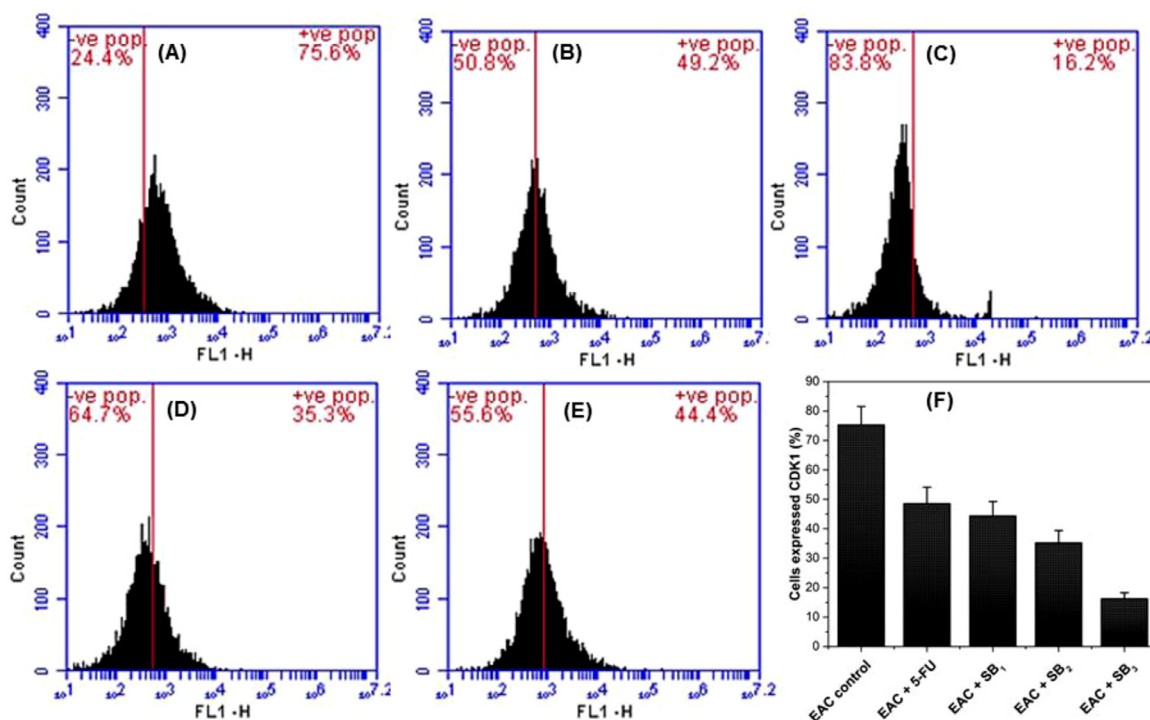


Fig. 6. Flow cytometric histogram showing; (A) Ehrlich control and the effect of (B) 5-Fu, (C) IVASB1, (D) IVASB2, and (E) IVASB3 on the expression of CDK1 in Ehrlich tumorized mice. (F) Effect of the tested compounds on CDK1 expression in Ehrlich cells.

arrest at G2/M-phase with respect to Ehrlich control which suggested that the two test compounds inhibit CDK1 expression.

### 3.9. Effect of tested compounds on PARP and VEGF

As shown in Table 4, the concentration of PARP in serum of tumorized mice received IVASB<sub>2</sub> and IVASB<sub>3</sub> decreased by 60% and

46.67% respectively, compared to Ehrlich control group ( $P \leq 0.01$ ). In the same way, the administration of IVASB<sub>2</sub> and IVASB<sub>3</sub> to tumorized mice decreased the concentration of VEGF in serum by 34.99% and 28.49% respectively, compared to Ehrlich control group ( $P \leq 0.001$ ).

PARP is considered the principal regulator for repairing damaged DNA [59], so that the inhibition of PARP in tumor cells de-

**Table 4**  
Effect of the tested compounds on PARP and VEGF in Ehrlich cells<sup>†</sup>.

Biomarkers	EAC control $M \pm SE$	Control $M \pm SE$	EAC + SB <sub>1</sub> $M \pm SE$	EAC + SB <sub>2</sub> $M \pm SE$	EAC + SB <sub>3</sub> $M \pm SE$	EAC +5-Fu $M \pm SE$
PARP (ng/mg)	1.5 ± 0.2	0.5***±0.02	1.07*±0.01	0.6**±0.2	0.8**±0.02	1.16*±0.02
VEGF (ng/mg)	84.6 ± 2.3	71.3***±1.2	74.8**±2.5	55***±1.5	60.5***±0.9	58.5***±1.1

<sup>†</sup> Values are represented as mean ±SE (n = 6), Where \* = Significant difference between test groups and Ehrlich control group, \*P ≤ 0.05.

\*\* P ≤ 0.01.

\*\*\* P ≤ 0.001.

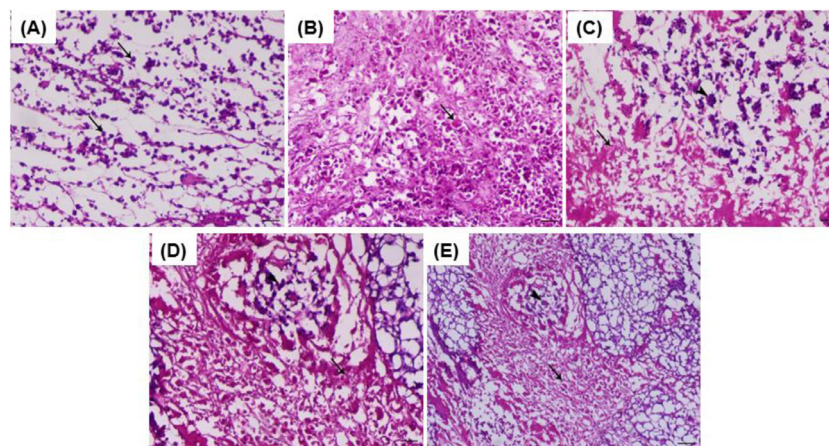


**Fig. 7.** Histopathological examination of Ehrlich solid tumor. Representative sections were obtained from (A) untreated Ehrlich control (Tumor mass showing wide proliferation of Ehrlich neoplastic cells of high mitotic figures (arrows), (B–D) Tumor mass of tumorized mice treated with IVASB<sub>1</sub>, IVASB<sub>2</sub>, and IVASB<sub>3</sub>, respectively, showing increase the degenerative and necrotic lesions with decrease the neoplastic cells (arrow) (E) Tumor mass of tumorized mice treated with 5-Fu showing increase the necrotic lesions (arrow) with decrease the neoplastic cells (arrowhead) Sections were stained with HE dyes (scale bar = 100 μm).

creases chemotherapy resistance and enhances treatment response [60]. In our investigation, all three test compounds inhibit PARP activity and the most potent inhibitor was found IVASB<sub>2</sub>. Furthermore, G<sub>0</sub>/G<sub>1</sub> cell cycle arrest caused by IVASB<sub>1</sub> and IVASB<sub>3</sub> indicated to the accumulation of DNA double-strand breaks, hence apoptosis induction.

VEGFs stimulate cancerous cells angiogenesis which means promoting the formation of new blood vessels to supply tumor mass with nutrients and oxygen. Therefore, the inhibition of VEGF is considered an efficient strategy in cancer treatment [61]. Based on our results, the test compounds significantly decreased the concentration of VEGF in the serum of Ehrlich-tumorized mice compared to Ehrlich control group. Several previous studies proved that thiazole Schiff base derivatives act as VEGFR-1 and 2 inhibitors [62].

### 3.10. Histopathological examination

The inoculation of Ehrlich tumor cells into the control mice induced intramuscular tumors at the point of inoculation. These tumors were prominent and revealed fast growth with mixed inflammatory reaction predominantly lymphocytes, white conglomerated mass and sometimes infiltrated into the muscle fibers of the animals. Examination of untreated tumorized mice presented that Ehrlich cells penetrated and mostly replaced the subcutaneous tissue with necrosis of the remaining skeletal muscles. Mice treated with 5-Fu revealed minimal tumor cell infiltrations, extensive necrosis, and apoptosis at the edge of the tumor with destructed blood vessels and depletion. Mice treated with IVASB<sub>1</sub>, IVASB<sub>2</sub>, and IVASB<sub>3</sub> (3.31 μg/kg, 55 mg/Kg and 450 mg/Kg, respectively) showed most necrosis with a decrease of the neoplastic cells (Fig. 7 (B–D)). There was a marked reduction in tumor size after treatment with the test compounds, the tumor was found to be intermittent and appeared growing slow and split. This indicates a partial prevention of the effects of EAC cells by test compounds.

## 4. Conclusion

In the present work, three novel hybrid thiazole-vanillyl and thiadiazole-vanillyl Schiff bases bearing imidazolium or lutidinium ionic liquids terminals (IVASBs) have successfully synthesized and structurally characterized based on their respective elemental and spectral (FTIR, NMR, and MS) analyses. They are coded as 3-(thiazol-2-ylimino)methylvanillyl-2-methylimidazolium chloride (IVASB<sub>1</sub>), 2,5-Bis-(5-(2-methylimidazolium chloride)-3-methoxysalicylideneimino)-1,3,4-thiadiazole (IVASB<sub>2</sub>), and 2,5-Bis-(5-(2,4-lutidinium chloride)-3-methoxysalicylidene-imino)-1,3,4-thiadiazole (IVASB<sub>3</sub>). The *in vitro* anti-breast cancer study revealed that IVASB<sub>1</sub> (IC<sub>50</sub> 13.5 ± 1.14 μg/mL) and IVASB<sub>3</sub> (IC<sub>50</sub> 3.73 ± 0.2 μg/mL) exhibited the highest ability to inhibit the proliferation of MCF-7 cells. These findings agreed with the molecular docking results. Flow-cytometric analysis showed that IVASBs significantly increased the percent of Ehrlich tumor cells undergoing sub G<sub>1</sub> phase and decreased the percent of cells in S phase, where IVASB<sub>3</sub> was the most effective. In addition, the administration of IVASB<sub>1</sub>, IVASB<sub>2</sub>, and IVASB<sub>3</sub> to tumorized mice caused a significant reduction in CDK1 expression by 41.27%, 53.31% and 78.57%, respectively compared to Ehrlich control group. Moreover, the concentrations of PARP and VEGF significantly decreased in serum of tumorized mice remediated by these compounds. Based on our results, IVASB<sub>3</sub> could act as a starting point for promising anti-breast cancer candidate, warrant further research and development.

### Declaration of Competing Interest

none

### CRediT authorship contribution statement

**Waleed M. Serag:** Supervision, Methodology, Data curation, Software, Validation, Writing – original draft, Writing – review

& editing. **Faten Zahran:** Supervision, Data curation, Validation, Visualization, Writing – original draft. **Yasmin M. Abdelghany:** Methodology, Data curation, Software, Visualization, Writing – original draft. **Reda F.M. Elshaarawy:** Conceptualization, Supervision, Methodology, Data curation, Validation, Writing – original draft, Writing – review & editing. **Moustafa S. Abdelhamid:** Supervision, Methodology, Software, Data curation, Validation, Writing – original draft, Writing – review & editing.

## Acknowledgement

The authors would like to thank Dr. Fatma H. A. Mustafa Marine Pollution Laboratory, Marine Environment Division, National Institute of Oceanography and Fisheries (NIOF), Suez, Egypt, for their generous efforts in supporting this work.

## Supplementary materials

Supplementary material associated with this article can be found, in the online version, at [doi:10.1016/j.molstruc.2021.131041](https://doi.org/10.1016/j.molstruc.2021.131041).

## References

- [1] E.A.L. Junior, A.S. Yamashita, G.D. Pimentel, L.G.O. De Sousa, R.V.T. Santos, C.L. Gonçalves, E.L. Streck, F.S. de Lira, J.C.R. Neto, Doxorubicin caused severe hyperglycaemia and insulin resistance, mediated by inhibition in AMPK signalling in skeletal muscle, *J. Cachexia Sarcopenia Muscle* 7 (2016) 615–625, doi:10.1002/jcsm.12104.
- [2] J.E. Klaunig, Z. Wang, X. Pu, S. Zhou, Oxidative stress and oxidative damage in chemical carcinogenesis, *Toxicol. Appl. Pharm.* 254 (2011) 86–99, doi:10.1016/j.taap.2009.11.028.
- [3] V. Asati, D.K. Mahapatra, S.K. Bharti, Thiazolidine-2, 4-diones as multi-targeted scaffold in medicinal chemistry: potential anticancer agents, *Eur. J. Med. Chem.* 87 (2014) 814–833, doi:10.1016/j.ejmech.2014.10.025.
- [4] K. Nikhil, S. Sharan, A.K. Singh, A. Chakraborty, P. Roy, Anticancer activities of pterostilbene-isothiocyanate conjugate in breast cancer cells: involvement of PPARgamma, *PLoS ONE* 9 (2014) e104592, doi:10.1371/journal.pone.0104592.
- [5] T.E. Sharp, J.C. George, Stem cell therapy and breast cancer treatment: review of stem cell research and potential therapeutic impact against cardiotoxicities due to breast cancer treatment, *Front. Oncol.* 4 (2014) 299, doi:10.3389/fonc.2014.00299.
- [6] M.L. Salem, N.M. Shoukry, W.K. Teleb, *In vitro* and *in vivo* antitumor effects of the Egyptian scorpion *Androctonus amoreuxi* venom in an Ehrlich ascites tumor model, *Springerplus* 5 (2016) 570, doi:10.1186/s40064-016-2269-3.
- [7] M. Feng, B. Tang, L.H. Liang, X. Jiang, Sulfur containing scaffolds in drugs: synthesis and application in medicinal chemistry, *Curr. Top. Med. Chem.* 16 (2016) 1200–1216.
- [8] P.K. Sharma, A. Amin, M. Kumar, A review: medicinally important nitrogen sulphur containing heterocycles, *Med. Chem. J.* 14 (2020) 49–64, doi:10.2174/1874104502014010049.
- [9] A.M. Borcea, I. Ionuț, O. Crișan, O. Oniga, An overview of the synthesis and antimicrobial, antiprotazoal, and antitumor activity of thiazole and bisthiazole derivatives, *Molecules* 26 (3) (2021) 624, doi:10.3390/molecules26030624.
- [10] Y. Wan, J. Long, H. Gao, Z. Tang, 2-Aminothiazole: a privileged scaffold for the discovery of anti-cancer agents, *Eur. J. Med. Chem.* 210 (2021) 112953, doi:10.1016/j.ejmech.2020.112953.
- [11] R.F.M. Elshaarawy, F.H.A. Mustafa, A.R. Sofy, A.A. Hmed, C. Janiak, A new synthetic antifouling coatings integrated novel aminothiazole-functionalized ionic liquids motifs with enhanced antibacterial performance, *J. Environ. Chem. Eng.* 7 (1) (2019) 102800–102810, doi:10.1016/j.jece.2018.11.044.
- [12] B.N. Ravi, J. Keshavayya, N.M. Mallikarjuna, V. Kumar, S. Kandgal, Synthesis, characterization and pharmacological evaluation of 2-aminothiazole incorporated azo dyes, *J. Mol. Struct.* 1204 (2020) 127493, doi:10.1016/j.molstruc.2019.127493.
- [13] N.S. Alahmadi, R.F.M. Elshaarawy, Novel aminothiazolyl-functionalized phosphonium ionic liquid as a scavenger for toxic metal ions from aqueous media; mining to useful antibiotic candidates, *J. Mol. Liq.* 281 (2019) 451–460, doi:10.1016/j.molliq.2019.01.154.
- [14] K.W. Jeong, J.H. Lee, S.M. Park, J.H. Choi, D.Y. Jeong, D.H. Choi, Y. Nam, J.H. Park, K.N. Lee, S.M. Kim, J.M. Ku, Synthesis and *in-vitro* evaluation of 2-amino-4-arylthiazole as inhibitor of 3D polymerase against foot-and-mouth disease (FMD), *Eur. J. Med. Chem.* 102 (2015) 387–397, doi:10.1016/j.ejmech.2015.08.020.
- [15] M. Modrić, M. Božičević, I. Faraho, M. Bosnar, I. Škorić, Design, synthesis and biological evaluation of new 1,3-thiazole derivatives as potential anti-inflammatory agents, *J. Mol. Struct.* 1239 (2021) 130526, doi:10.1016/j.molstruc.2021.130526.
- [16] E. Khan, A. Khan, Z. Gul, et al., Molecular salts of terephthalic acids with 2-aminopyridine and 2-aminothiazole derivatives as potential antioxidant agents; Base-acid-base type architectures, *J. Mol. Struct.* 1200 (2020) 127126, doi:10.1016/j.molstruc.2019.127126.
- [17] G. Turan-Zitouni, P. Chevallet, F.S. Kiliç, K. Erol, Synthesis of some thiazolyl-pyrazoline derivatives and preliminary investigation of their hypotensive activity, *Eur. J. Med. Chem.* 35 (2000) 635–641, doi:10.1016/S0223-5234(00)00152-5.
- [18] N. Siddiqui, W. Ahsan, Synthesis, anticonvulsant and toxicity screening of thiazolyl-thiadiazole derivatives, *Med. Chem. Res.* 20 (2011) 261–268, doi:10.1007/s00044-010-9313-6.
- [19] M. Pieroni, B. Wan, S. Cho, S.G. Franzblau, G. Costantino, Design, synthesis and investigation on the structure-activity relationships of *N*-substituted 2-aminothiazole derivatives as antitubercular agents, *Eur. J. Med. Chem.* 72 (2014) 26–34, doi:10.1016/j.ejmech.2013.11.007.
- [20] O. Özbek, M.B. Gürdere, Synthesis and anticancer properties of 2-aminothiazole derivatives, *Phosphorus Sulfur Silicon Relat. Elem.* 196 (5) (2021) 444–454, doi:10.1080/10426507.2020.1871347.
- [21] J. Matysiak, Biological and pharmacological activities of 1,3,4-thiadiazole based compounds, *Mini Rev. Med. Chem.* 15 (9) (2015) 762–775, doi:10.2174/1389557515666150519104057.
- [22] M. Szeliga, Thiadiazole derivatives as anticancer agents, *Pharmacol. Rep.* 72 (2020) 1079–1100, doi:10.1007/s43440-020-00154-7.
- [23] S. Janowska, A. Paneth, M. Wujec, Cytotoxic properties of 1,3,4-thiadiazole derivatives—a review, *Molecules* 25 (18) (2020) 4309, doi:10.3390/molecules25184309.
- [24] A. Hameed, M. al-Rashida, M. Uroos, S.A. Ali, K.M. Khan, Schiff bases in medicinal chemistry: a patent review (2010–2015), *Expert Opin. Ther. Pat.* 27 (1) (2017) 63–79, doi:10.1080/13543776.2017.1252752.
- [25] G. Matela, Schiff bases and complexes: a review on anti-cancer activity, *Anticancer Agents Med. Chem.* 20 (10) (2020) 1908–1917, doi:10.2174/1871520620666200507091207.
- [26] S. Sowmia, C.I. Cheng, Y.H. Chu, Ionic liquids for green organic synthesis, *Curr. Org. Synth.* 9 (2012) 74–95, doi:10.2174/15701791279889116.
- [27] V.V. Singh, A.K. Nigam, A. Batra, M. Boopathi, B. Singh, R. Vijayaraghavan, Applications of ionic liquids in electrochemical sensors and biosensors, *Int. J. Electrochem.* 19 (2012) 165683, doi:10.1155/2012/165683.
- [28] V. Pino, M. Germán-Hernández, A. Martín-Pérez, J.L. Anderson, Ionic liquid-based surfactants in separation science, *Sep. Sci. Technol.* 47 (2012) 264–276, doi:10.1080/01496395.2011.620589.
- [29] K.S. Egorova, E.G. Gordeev, V.P. Ananikov, Biological activity of ionic liquids and their application in pharmaceuticals and medicine, *Chem. Rev.* 117 (2017) 7132–7189, doi:10.1021/acs.chemrev.6b00562.
- [30] P.R.V. Rao, K.A. Venkatesan, A. Rout, Potential applications of room temperature ionic liquids for fission products and actinide separation, *Sep. Sci. Technol.* 47 (2012) 204–222, doi:10.1080/01496395.2011.628733.
- [31] S.M. Saleh, R. Ali, R.F.M. Elshaarawy, A ratiometric and selective fluorescent chemosensor for Ca(II) ions based on a novel water-soluble ionic Schiff-base, *RSC Adv.* 6 (2016) 68709–68718, doi:10.1039/C6RA12750A.
- [32] R.F.M. Elshaarawy, R. Ali, S.M. Saleh, C. Janiak, A novel water-soluble highly selective “switch-on” ionic liquid-based fluorescent chemi-sensor for Ca (II), *J. Mol. Liq.* 241 (2017) 308–315, doi:10.1016/j.molliq.2017.06.016.
- [33] R.F.M. Elshaarawy, W.A. Mokbel, E.A. El-Sawi, Novel ammonium ionic liquids as scavengers for aromatic and heterocyclic amines: conversion into new pharmacological agents, *J. Mol. Liq.* 223 (2016) 1123–1132, doi:10.1016/j.molliq.2016.09.042.
- [34] W.N. El-Sayed, J. Alkabli, K. Althumayri, R.F.M. Elshaarawy, L.A. Ismaile, Azomethine-functionalized task-specific ionic liquid for diversion of toxic metal ions in the aqueous environment into pharmacological nominates, *J. Mol. Liq.* 322 (2021) 114525, doi:10.1016/j.molliq.2020.114525.
- [35] S. Mishra, A.K. Tamta, M. Sarikhani, P.A. Desingu, S.M. Kizkekra, A.S. Pandit, S. Kumar, D. Khan, S.C. Raghavan, N.R. Sundaresan, Subcutaneous Ehrlich ascites carcinoma mice model for studying cancer-induced cardiomyopathy, *Sci. Rep.* 8 (2018) 5599, doi:10.1038/s41598-018-23669-9.
- [36] A. Khamis, M.A. El-Magd, S.K. NasrEldien, Toxicity studies of trehalose and/or methotrexate in mice, *Res. J. Pharm. Biol. Chem. Sci.* 9 (2018) 83–89.
- [37] C. Sánchez-Martínez, L.M. Gelbert, M.J. Lallena, A. de Dio, Cyclin Dependent Kinase (CDK) inhibitors as anticancer drugs, *Bioorg. Med. Chem. Lett.* 25 (17) (2015) 3420–3435, doi:10.1016/j.bmcl.2015.05.100.
- [38] G. de Cárcer, I.P. de Castro, M. Malumbres, Targeting cell cycle kinases for cancer therapy, *Curr. Med. Chem.* 14 (2007) 969–985, doi:10.2174/092986707780362925.
- [39] U. Asghar, A.K. Witkiewicz, N.C. Turner, E.S. Knudsen, The history and future of targeting cyclin-dependent kinases in cancer therapy, *Nat. Rev. Drug Discov.* 14 (2015) 130–146, doi:10.1038/nrd4504.
- [40] Y. Zeng, S. Stauffer, J. Zhou, X. Chen, Y. Chen, J. Dong, Cyclin-dependent kinase 1 (CDK1)-mediated mitotic phosphorylation of the transcriptional co-repressor Vgll4 inhibits its tumor-suppressing activity, *J. Biol. Chem.* 292 (2017) 15028–15038, doi:10.1074/jbc.M117.796284.
- [41] A.R. Sofy, A.A. Hmed, N.F.A. El Halim, M.A.E. Zein, R.F.M. Elshaarawy, Polyphosphonium-oligochitosans decorated with nanosilver as new prospective inhibitors for common human enteric viruses, *Carbohydr. Polym.* 226 (2019) 115261, doi:10.1016/j.carbpol.2019.115261.
- [42] R.F.M. Elshaarawy, I.M. Eldeen, E.M. Hassan, Efficient synthesis and evaluation of bis-pyridinium/bis-quinolinium metallosalophens as antibiotic and anti-tumor candidates, *J. Mol. Struct.* 1128 (2017) 162–173, doi:10.1016/j.molstruc.2016.08.059.

- [43] R.F.M. Elshaarawy, C. Janiak, Antibacterial susceptibility of new copper(II) N-pyruvoyl anthranilate complexes against marine bacterial strains-in search of new antibiofouling candidate, *Arab. J. Chem.* 9 (6) (2016) 825–834, doi:[10.1016/j.arabjc.2015.04.010](https://doi.org/10.1016/j.arabjc.2015.04.010).
- [44] M.Y. Alfaifi, S.E.I. Elbehairi, H.S. Hafez, R.F.M. Elshaarawy, Spectroscopic exploration of binding of new imidazolium-based palladium (II) saldach complexes with CT-DNA as anticancer agents against HER2/neu overexpression, *J. Mol. Struct.* 1191 (2019) 118–128, doi:[10.1016/j.molstruc.2019.04.119](https://doi.org/10.1016/j.molstruc.2019.04.119).
- [45] L.J. Reed, H. Muench, A simple method of estimating fifty percent endpoints, *Am. J. Epidemiol.* 27 (3) (1938) 493–497.
- [46] E. Noaman, N.K.B. El-Din, M.A. Bibars, Antioxidant potential by arabinoxylan rice bran, MGN-3/biobran, represents a mechanism for its oncogenic effect against murine solid Ehrlich carcinoma, *Cancer Lett.* 268 (2) (2008) 348–359, doi:[10.1016/j.canlet.2008.04.012](https://doi.org/10.1016/j.canlet.2008.04.012).
- [47] N. Orsolich, Z. Tadic, V. Benkovic, A. Horvat, D. Lisičić, I. Bašić, Basic I Stimulation of hematopoiesis by a water-soluble derivative of propolis in mice, *Pharmacologyonline* 3 (2006) 698–705.
- [48] E. Frankenberg, Influence of light and temperature on daily activity patterns of three Israeli forms of *Ptyodactylus*, *J. Zool.* 189 (1979) 21–30, doi:[10.1111/j.1469-7998.1979.tb03950.x](https://doi.org/10.1111/j.1469-7998.1979.tb03950.x).
- [49] R.F.M. Elshaarawy, Y. Lan, C. Janiak, Oligonuclear homo- and mixed-valence manganese complexes based on thiophene- or aryl-carboxylate ligation: synthesis, characterization and magnetic studies, *Inorg. Chim. Acta* 401 (2013) 85–94, doi:[10.1016/j.ica.2013.03.019](https://doi.org/10.1016/j.ica.2013.03.019).
- [50] R.F.M. Elshaarawy, F.H.A. Mustafa, A.R. Sofy, A.A. Hmed, C. Janiak, A new synthetic antifouling coatings integrated novel aminothiazole-functionalized ionic liquids motifs with enhanced antibacterial performance, *J. Environ. Chem. Eng.* 7 (1) (2019) 102800–102810, doi:[10.1016/j.jece.2018.11.044](https://doi.org/10.1016/j.jece.2018.11.044).
- [51] R.F.M. Elshaarawy, H.R.Z. Tadros, R.M. Abd El-Aal, F.H.A. Mustafa, Y.A. Soliman, M.A. Hamed, Hybrid molecules comprising 1,2,4-triazole or diaminothiadiazole Schiff-bases and ionic liquid moieties as potent antibacterial and marine antibiofouling nominees, *J. Environ. Chem. Eng.* 4 (3) (2016) 2754–2764, doi:[10.1016/j.jece.2016.05.016](https://doi.org/10.1016/j.jece.2016.05.016).
- [52] R.F.M. Elshaarawy, J. Dechnik, H.M.A. Hassan, D. Dietrich, M.A. Betiha, S. Schmidt, C. Janiak, Novel high throughput mixed matrix membranes embracing poly ionic liquid-grafted biopolymer: fabrication, characterization, permeation and antifouling performance, *J. Mol. Liq.* 266 (2018) 484–494, doi:[10.1016/j.molliq.2018.06.100](https://doi.org/10.1016/j.molliq.2018.06.100).
- [53] S. Lim, P. Kaldis, Cdks, cyclins and CKIs: roles beyond cell cycle regulation, *Development* 140 (2013) 3079–3093, doi:[10.1242/dev.091744](https://doi.org/10.1242/dev.091744).
- [54] R. Roskoski, Cyclin-dependent protein kinase inhibitors including palbociclib as anticancer drugs, *Pharmacol. Res.* 107 (2016) 249–275, doi:[10.1016/j.phrs.2016.03.012](https://doi.org/10.1016/j.phrs.2016.03.012).
- [55] A. Satyanarayana, P. Kaldis, Mammalian cell-cycle regulation: several Cdks, numerous cyclins and diverse compensatory mechanisms, *Oncogene* 28 (2009) 2925–2939, doi:[10.1038/onc.2009.170](https://doi.org/10.1038/onc.2009.170).
- [56] Z. Wang, A. Slipicevic, M. Forsund, C.G. Trope, J.M. Nesland, R. Holm, Expression of CDK1(Tyr15), pCDK1(Thr161), Cyclin B1 (total) and pCyclin B1(Ser126) in vulvar squamous cell carcinoma and their relations with clinicopathological features and prognosis, *PLoS ONE* 10 (2015) e0121398, doi:[10.1371/journal.pone.0121398](https://doi.org/10.1371/journal.pone.0121398).
- [57] P. Oliva, V. Onnis, E. Balboni, E. Hamel, F. Estévez-Sarmiento, J. Quintana, F. Estévez, A. Brancale, S. Ferla, S. Manfredini, R. Romagnoli, Synthesis and biological evaluation of 2-substituted benzyl-/phenylethylamino-4-amino-5-arylothiazoles as apoptosis-inducing anticancer agents, *Molecules* 25 (9) (2020) 2177, doi:[10.3390/molecules25092177](https://doi.org/10.3390/molecules25092177).
- [58] R. Romagnoli, P.G. Baraldi, M.D. Carrion, O. Cruz-Lopez, C.L. Cara, G. Basso, G. Viola, M. Khedr, J. Balzarini, S. Mahboobi, A. Sellmer, A. Brancale, E. Hamel, 2-arylamino-4-amino-5-arylothiazoles. “One-pot” synthesis and biological evaluation of a new class of inhibitors of tubulin polymerization, *J. Med. Chem.* 52 (17) (2009) 5551–5555, doi:[10.1021/jm9001692](https://doi.org/10.1021/jm9001692).
- [59] A. Sonnenblick, E. de Azambuja, H.A. Azim, M. Piccart, An update on PARP inhibitors-moving to the adjuvant setting, *Nat. Rev. Clin. Oncol.* 12 (2014) 27–41, doi:[10.1038/nrclinonc.2014.163](https://doi.org/10.1038/nrclinonc.2014.163).
- [60] C.J. Lord, A. Ashworth, PARP inhibitors: synthetic lethality in the clinic, *Science* 355 (2017) 1152–1158, doi:[10.1126/science.aam7344](https://doi.org/10.1126/science.aam7344).
- [61] M. Perrot-Appianat, M. Di Benedetto, Autocrine functions of VEGF in breast tumor cells: adhesion, survival, migration and invasion, *Cell Adhes. Migr.* 6 (6) (2012) 547–553, doi:[10.4161/cam.23332](https://doi.org/10.4161/cam.23332).
- [62] S.M. Abou-Seri, W.M. Eldehna, M.M. Ali, 1-piperazinylphthalazines as potential VEGFR-2 inhibitors and anticancer agents: synthesis and *in vitro* biological evaluation, *Eur. J. Med. Chem.* 107 (2016) 165–179, doi:[10.1016/j.ejmech.2015.10.053](https://doi.org/10.1016/j.ejmech.2015.10.053).